The application of the monoclinic BiB_3O_6 nonlinear crystal in ultrafast laser technology

Valentin Petrov,[a)] Alexander Gaydardzhiev,[b)] Ivailo Nikolov,[b)]
Ivan Buchvarov,[b)] Pancho Tzankov,[a,♦)] Frank Noack[a)]

[a]Max-Born-Institute for Nonlinear Optics and Ultrafast Spectroscopy, 2A Max-Born-Str., D-12489 Berlin, Germany;
[b]Department of Physics, Sofia University, 5 James Bourchier Blvd., BG-1164 Sofia, Bulgaria

ABSTRACT

BiB_3O_6 (BIBO), the first low-symmetry (monoclinic class 2) inorganic nonlinear crystal that became commercially available, possesses some unique advantages for applications in ultrafast laser technology which are primarily related to its dispersive properties. In the present paper, these properties are analyzed in more detail and compared with other crystals. Of special interest is the pumping of this material near 800 nm for broadband parametric amplification in the near-infrared between 1.15 and 2.4 μm. We present experimental results on generation and amplification of ultrabroadband femtosecond continua in this spectral range using amplified Ti:sapphire lasers as pump sources.

Key words: optical parametric generators and amplifiers; broadband gain; bismuth triborate; femtosecond pulses

1. INTRODUCTION

A combination of attractive properties makes bismuth triborate, BiB_3O_6 (BIBO), a promising material for frequency conversion using phase-matched second-order nonlinear processes. This is the first inorganic crystal with such low symmetry (monoclinic, point group 2) which became commercially available. As a biaxial crystal it offers versatile phase-matching configurations which are extended by the low symmetry to additional interactions (e.g. positive and negative type in the same principal plane) with non-vanishing effective nonlinearity which has to be considered in two independent octants.[1] For a borate compound, BIBO exhibits exceptionally high second order nonlinear susceptibility[2] which is associated with the contribution of the BiO_4 anionic group.[3] As a matter of fact, the effective nonlinearity of BIBO can be larger than that of $KTiOPO_4$ (KTP), d_{eff}(KTP)<2.65 pm/V, while the lower transparency edge extends deeper into the UV (286 nm).[4] The above, together with the high optical damage threshold, as in β-BaB_2O_4 (BBO) and LiB_3O_5 (LBO), make BIBO very suitable for application in ultrafast laser technology because dispersion effects can be reduced by simply choosing a correspondingly shorter crystal length. Several papers reviewing the ultrafast frequency conversion schemes, already realized with BIBO, appeared recently.[5,6,7] Previous applications in the femtosecond domain include efficient second harmonic generation (SHG) using tunable pulses near 800 nm from high repetition rate mode-locked Ti:sapphire lasers[7-10] and 1 kHz Ti:sapphire amplifiers,[10] as well as SHG of a synchronously pumped optical parametric oscillator (SPOPO) emitting between 620 and 710 nm,[11] femtosecond SPOPO pumped at 415 nm and operating at 76 MHz between 480 and 710 nm (signal wave),[5,7,12] an analogous SPOPO pumped at 840 nm and operating between 1200 and 1600 nm for the signal wave,[13] and high energy femtosecond optical parametric amplifiers (OPAs) pumped near 800 nm and operating at 1 kHz between 1085 and 3050 nm (signal and idler).[6,14,15] Obviously, the fact that the absorption edge of BIBO is below 300 nm makes this crystal very suitable for pumping with short pulses in the 800 nm spectral range, using ultrafast Ti:sapphire laser systems, because two-photon absorption can be avoided. Moreover, the dispersive properties of BIBO, as demonstrated in the OPA arrangement utilizing type-I interaction,[15] are very suitable for broadband parametric amplification using pump wavelengths in the 800 nm spectral range. In this work

♦ Current affiliation: Quantronix Corporation, 41 Research Way, East Setauket, NY 11733, USA.

Nonlinear Frequency Generation and Conversion: Materials, Devices, and Applications VII, edited by Peter E. Powers,
Proc. of SPIE Vol. 6875, 68750X, (2008) · 0277-786X/08/$18 · doi: 10.1117/12.761019

we will analyze these properties in more detail, comparing with some other widely spread nonlinear materials, and present experimental results on ultrabroadband parametric amplification and generation of femtosecond white light continuum (WLC) using type-I BIBO crystals operated near degeneracy and pumped by amplified femtosecond pulses near 800 nm from 1 kHz Ti:sapphire laser systems.

2. PHASE-MATCHING PROPERTIES OF BIBO FOR OPA

As a monoclinic crystal with point group 2, BIBO is optically biaxial which offers a greater variety of phase-matching configurations in comparison to BBO. For OPA pumped near 800 nm, all these phase-matching configurations occur in the x-z principal plane (φ=0°). Table 1 shows the calculated phase-matching angles, inverse group-velocity mismatch (GVM) parameters and effective nonlinearity for a pump wavelength of λ_P=800 nm and a signal wavelength of λ_S=1400 nm.

Table 1. Phase-matching configurations and their characteristics for BIBO-OPA pumped near 800 nm.

interaction	θ [°]	$1/v_P$-$1/v_S$ [fs/mm]	$1/v_S$-$1/v_I$ [fs/mm]	d_{eff} [pm/V]
e→oo	11.03	4.5	-2.4	3.14
o→ee	35.15	35.0	1.3	1.56
o→eo	42.04	-28.7	126	2.38
o→oe	46.86	100	-175	2.19

The Sellmeier equations used to calculate the phase-matching angle θ and the group velocities of the pump, signal and idler waves (v_P, v_S, ad v_I) are those recently refined[16] but for calculating the effective nonlinearity d_{eff} ($d_{eff}=d_{12}\cos\theta$ for e→oo, o→eo, and o→oe interaction and $d_{eff}=d_{14}\sin 2\theta$ for o→ee interaction) we used averaged values for the nonlinear coefficients to account for Kleinman symmetry, as specified elsewhere.[1] The GVM between the signal and idler waves gives an idea about the expected gain bandwidth while the GVM between the pump and signal waves is an indication for the effective interaction length with the pump and hence for the efficiency of the conversion process. It is clear from Table 1 that although both type-I interaction processes will be characterized by large parametric gain bandwidths, the negative type phase-matching e→oo ensures two times higher effective nonlinearity and better temporal overlap with the pump. Similar arguments make the o→eo configuration preferable from the two type-II phase-matching schemes.

The most important advantage of type-II interaction is the possibility to tune, even close to degeneracy, with almost constant signal and idler bandwidths which enables the generation of bandwidth-limited pulses. Type-I interaction is advantageous for seeded OPAs, i.e. as a second stage when the first stage determines the final bandwidth of the amplified pulses. In addition, what is most important for the present work, type-I interaction is very attractive for generation and amplification of broadband continua by optical parametric generators (OPGs) or OPAs, and production of ultimately short pulses in the near-IR, even down to the single-cycle regime. Type-I e→oo interaction in BIBO is characterized by almost constant effective nonlinearity (<3% changes in the whole tuning range). In the following considerations we will focus mostly on this type of interaction in BIBO since it was the one realized in the experiments described later.

From Fig. 1a it can be seen that for both type-I interactions, the GVM between the signal and idler of an 800 nm pumped OPA based on BIBO vanishes when degeneracy is approached as could be expected. However, there is quite a broad spectral range only for the case of e→oo interaction, between λ_S=1300 nm and 1400 nm, where the signal and idler pulses travel with group velocities which are very close to that of the pump, the one faster and the other slower than the pump. This is very advantageous for efficient parametric amplification in the presence of GVM.[17] In fact at longer signal wavelengths, up to degeneracy, the interaction length with the pump is much longer for type e→oo than for type o→ee phase-matching. Thus, it is obvious from Table 1 and Fig. 1a that e→oo type BIBO is ideal for broadband parametric amplification in collinear geometry exactly when the pump wavelength is near 800 nm. Second order terms (group velocity dispersion, GVD) have to be taken into account near degeneracy. However, calculations show that in the case of type-I BIBO, even the GVD approximation is violated.

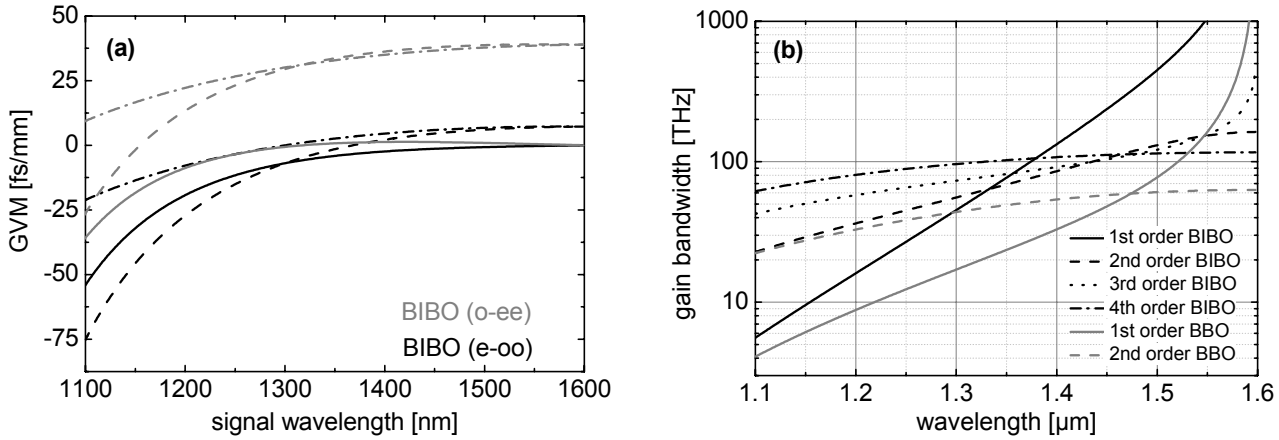

Fig. 1. (a) Inverse group velocity mismatch (GVM) between the pump and idler ($1/v_P$-$1/v_I$, dashed lines), between the pump and signal ($1/v_P$-$1/v_S$, dash-dotted lines), and between the signal and idler ($1/v_S$-$1/v_I$, solid lines) in type-I, e→oo (black curves) and o→ee (grey curves) interaction in BIBO for λ_P=800 nm, and (b) Gain bandwidth (FWHM) of BIBO and BBO, analytically calculated for collinear type e→oo interaction at λ_P=800 nm, a crystal length of 5 mm and pump intensity of 50 GW/cm^2 using only the first, second, third and fourth order Taylor series expansion terms of the wave-vector mismatch Δk, respectively.

In the plane-wave approximation, in the absence of pump depletion, the steady state gain for the signal wave (intensity) is given by:[17,18]

$$G = 1 + \frac{\Gamma^2}{g^2} sinh^2(gL) \tag{1}$$

with $g = \sqrt{\Gamma^2 - (\Delta k/2)^2}$ where $\Delta k = k_S + k_I - k_P$ is the wave mismatch and the exponential gain coefficient Γ is defined by $\Gamma^2 = \frac{8\pi^2 d_{eff}^2 I_P}{n_P n_S n_I \lambda_I \lambda_S \varepsilon_0 c}$. In the large gain ($\Gamma L >> 1$) limit the above equation simplifies to:

$$G = \frac{1}{4} exp(2gL) \tag{2}$$

In order to obtain analytical expressions for the parametric gain bandwidth, the wave mismatch is usually expanded in series as a function of the frequency, assuming in a first approximation that the pump is monochromatic,

$$\Delta k = \Delta k_0 + \left(\frac{\partial k_S}{\partial \omega_S} - \frac{\partial k_I}{\partial \omega_I}\right)\Delta\omega + \frac{1}{2!}\left(\frac{\partial^2 k_S}{\partial \omega_S^2} + \frac{\partial^2 k_I}{\partial \omega_I^2}\right)(\Delta\omega)^2 + \frac{1}{3!}\left(\frac{\partial^3 k_S}{\partial \omega_S^3} - \frac{\partial^3 k_I}{\partial \omega_I^3}\right)(\Delta\omega)^3 + \frac{1}{4!}\left(\frac{\partial^4 k_S}{\partial \omega_S^4} + \frac{\partial^4 k}{\partial \omega_I^4}\right)(\Delta\omega)^4 \ldots \tag{3}$$

The phase-matching condition means that Δk_0=0. In the above expression, $\Delta\omega = \Delta\omega_S$ denotes the frequency change of the signal wave and by energy conservation the idler frequency change will be $\Delta\omega_I = -\Delta\omega$. The individual terms in Eq. (3) are used to evaluate the points, in terms of frequency, where the gain function G from Eq. (2) drops to 50% of its maximum value. The results when using the first derivative (GVM approximation) and the second derivative (GVD approximation) are well known[17,18] and read, in terms of FWHM for $\Delta\nu = \Delta\omega/2\pi$:

$$\Delta\nu = \frac{2(ln\,2)^{1/2}}{\pi}\left(\frac{\Gamma}{L}\right)^{1/2}\left|\frac{1}{v_S} - \frac{1}{v_I}\right|^{-1} \tag{4}$$

$$\Delta\nu = \frac{2(ln2)^{1/4}}{\pi}\left(\frac{\Gamma}{L}\right)^{1/4}\left|\frac{\partial^2 k_S}{\partial\omega_S^2}+\frac{\partial^2 k_I}{\partial\omega_I^2}\right|^{-1/2} \tag{5}$$

Considering the next terms one obtains from Eqs. (2) and (3):

$$\Delta\nu = \frac{(144\,ln2)^{1/6}}{\pi}\left(\frac{\Gamma}{L}\right)^{1/6}\left|\frac{\partial^3 k_S}{\partial\omega_S^3}-\frac{\partial^3 k_I}{\partial\omega_I^3}\right|^{-1/3} \tag{6}$$

$$\Delta\nu = \frac{2(9\,ln2)^{1/8}}{\pi}\left(\frac{\Gamma}{L}\right)^{1/8}\left|\frac{\partial^4 k_S}{\partial\omega_S^4}+\frac{\partial^4 k_I}{\partial\omega_I^4}\right|^{-1/4} \tag{7}$$

It is clear that for collinear type-I interaction the third order term, Eq. (6), also vanishes near degeneracy and this makes it necessary to consider the fourth order term,[19] which is given by Eq. (7). From the four approximations, one should use, depending on the signal wavelength, the one which predicts the smallest gain bandwidth. In the λ_S=1100-1300 nm range for e→oo phase-matching in the x-z plane of BIBO pumped at 800 nm, this is the solution based on the GVM term. Approaching degeneracy, however, the GVD term also vanishes which is a consequence of the fact that for polarization parallel to the y-axis (o-wave for the present interaction scheme), it is zero at 1580 nm. It is interesting that, as can be seen from Fig. 1b, the fourth order approximation should be used starting already from 1500 nm. This approximation predicts a gain bandwidth (FWHM intensity) of the order of about 3800 cm^{-1} (116 THz) near degeneracy. In contrast, the spectral bandwidth of BBO (same type e→oo phase-matching) for the same crystal and pump parameters is determined near degeneracy by the second order derivatives and amounts to 63 THz, i.e. it is roughly two times smaller, see Fig. 1b.

Direct calculations of the parametric gain G using Eq. (1) at the exact phase-matching angle are presented in Fig. 2a. In can be seen that the gain bandwidth at first increases but then decreases with the pump wavelength. There exists an optimum pump wavelength near λ_P=780 nm where the gain bandwidth is maximized, as can be seen in Fig. 2b where the grey area depicts the range limited by the ½ drop of the gain from its maximum value. The left part of the figure corresponds to the retracing behavior of the phase-matching curves, see Fig. 2c, where "satellites" appear in Fig. 2a, corresponding to the second pair of signal and idler waves phase-matched at the same angle θ.

Thus, collinear e→oo interaction in BIBO possesses for pump wavelengths near 800 nm the exclusive property of simultaneous vanishing of the first three terms that determine the gain bandwidth. Many other nonlinear crystals with sufficient birefringence possess in fact the same property provided the three wavelengths lie within the transparency range. This is related to the existence of retracing behavior of the phase-matching curves[19,20] which can be traced back to the material dispersive properties. In any case, it happens at a certain pump wavelength which does not necessarily coincide with the wavelengths of the available powerful femtosecond laser sources that can be used for pumping an OPA or OPG. As can be seen from Table 2 this same property is characteristic also of periodically poled materials (Type-0 interaction) where quasi-phase-matching is realized by suitable choice of the period. Note that retracing behavior (and the gain bandwidth) can be controlled also by changing the crystal temperature, see the computed curves in Fig. 2c.

Moreover, there is another favourable property related to the dispersion characteristics of BIBO which directly affects the interaction length with the pump and consequently the achievable conversion efficiency. The retracing behavior occurs at phase-matching angles for which the corresponding curves reverse their curvature as a function of the pump wavelength, see Fig. 2c. The critical angle for which this happens in type-I (e→oo) BIBO is in the vicinity of the turning point of the phase-matching curve for the inverse process, second harmonic generation (SHG). Such a turning point in the dependence of the fundamental wavelength on the phase-matching angle in SHG means nothing but broadband SHG phase-matching which is equivalent to vanishing GVM between the fundamental and the second harmonic. Indeed, it can be easily shown that this GVM vanishes at the point where $(\partial\theta/\partial\lambda)_{\lambda_F}=0$ for the SHG phase-matching curve,[21] see Fig. 2c. The existence of a turning point in the SHG phase-matching curve, which is attributed to anomalous

dispersion,[21] determines in fact the existence of the retracing phenomenon in the OPA/OPG curves, which can be characterized by three or more turning points.[20] This can be easily seen from Fig. 2c but the origin of the phenomenon can be traced back to the refractive index dependences, shown for BIBO in Fig. 3.

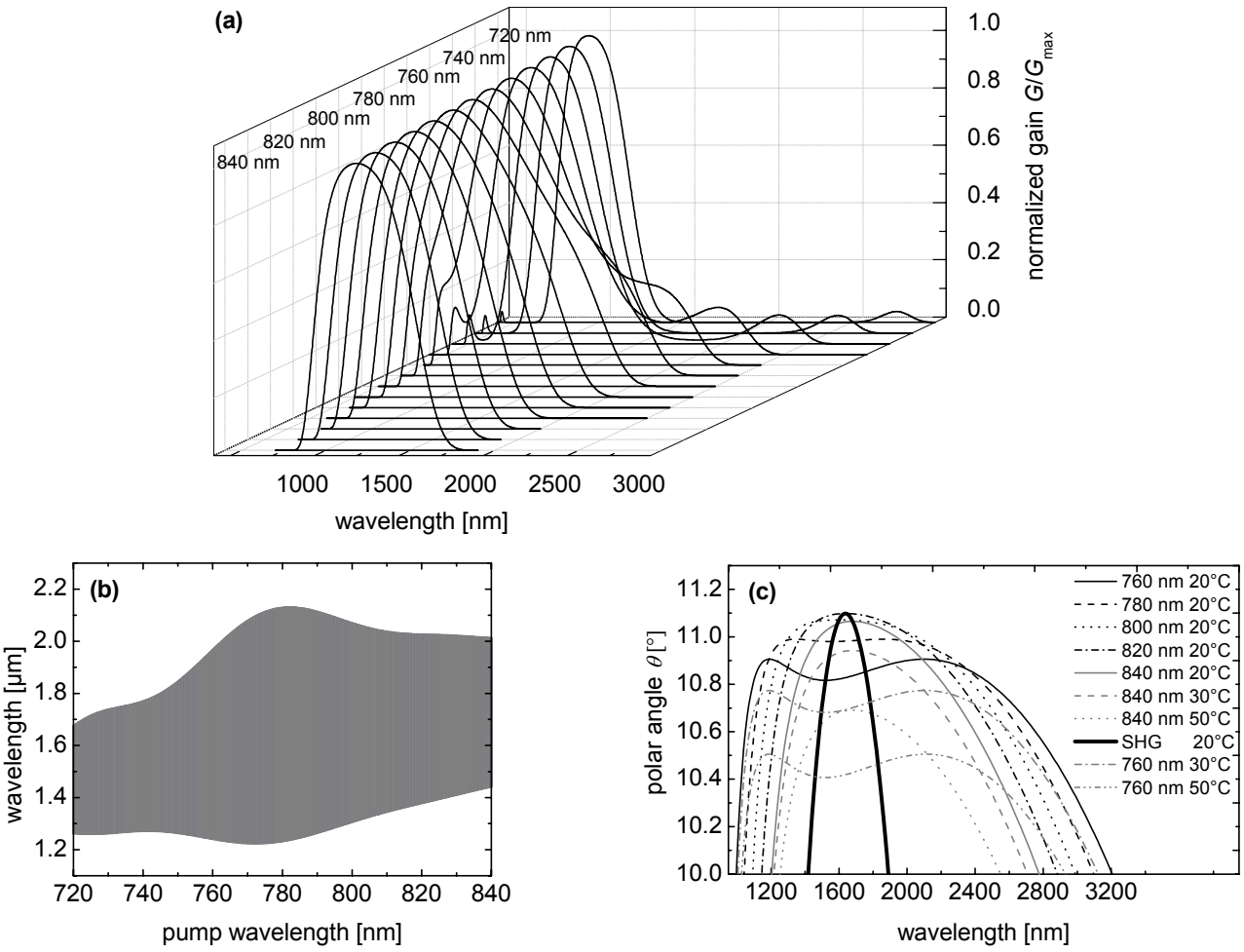

Fig. 2. (a) Normalized parametric gain in BIBO (negative type-I e→oo interaction in the x-z plane) calculated at exact phase-matching angles for different pump wavelengths (indicated), a crystal length of 5 mm and pump intensity of 50 GW/cm^2, (b) gain bandwidth as estimated from (a) at ½ level for the intensity, (c) phase-matching curves at different pump wavelengths and crystal temperatures (indicated) for the same process and SHG type-I (oo→e) at room temperature. The absolute gain G for (a) decreases from 1.41×10^8 at λ_P=720 nm to 2.91×10^7 at λ_P=780 nm and to 5.56×10^6 at λ_P=840 nm.

Although similar analytical relations cannot be derived for the GVM with the pump in the case of three waves (because both the signal and idler are broadband), it is clear that an OPA/OPG operating in the vicinity of the phase-matching angle where the SHG phase-matching curve has a turning point will be also characterized by very low GVM between the pump and the other two waves. For example, for the considered type of interaction in BIBO, the turning point of the SHG phase-matching curve occurs at a fundamental wavelength of λ_F=1637 nm. Both this wavelength and the "magic" pump wavelength for ultrabroadband parametric amplification were calculated and are presented in Table 2 for several crystals applicable in the near-IR. In the other type-I interaction scheme (o→ee phase-matching) in BIBO the deviation of λ_F from $2\lambda_P$ is larger and consequently the GVM with the pump is also larger, see Fig. 1a. In fact, Table 1 shows that the only crystal for which the GVM with the pump at λ_P is smaller than for e→oo type BIBO, is CLBO.

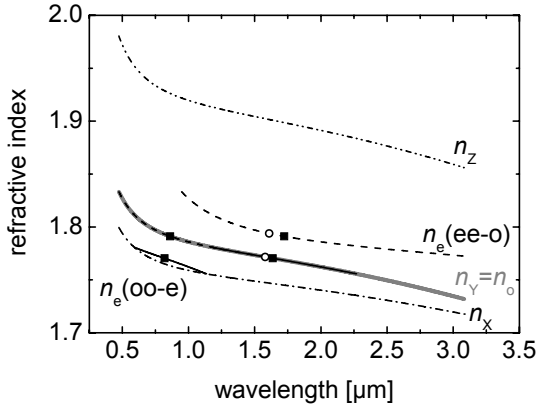

Fig. 3. Refractive index of BIBO for type-I SHG in the x-z plane. The wavelength ranges are determined by the validity of the Sellmeier expansions used (474-3083 nm).[16] Solid curves correspond to oo→e and dashed curves to ee→o phase-matching. The squares indicate the points where the first derivatives of the refractive index for the fundamental and second harmonic are equal (broadband SHG phase-matching corresponding to λ_F in Table 2) and the circles indicate the points of vanishing second derivative (corresponding to twice the "magic" pump wavelength or $2\lambda_P$ in Table 2).

Table 2. Parameters of several crystals that can be used in ultrabroadband OPA/OPG schemes pumped below 1 μm: λ_P is the "magic" pump wavelength for which the signal/idler GVD vanishes near degeneracy; λ_F is the fundamental wavelength for broadband SHG, $\Delta\lambda/\Delta\nu$ correspond to the wavelength / frequency range for maximum gain bandwidth calculated at the 1/2 level (crystal length 5 mm, pump intensity 50 GW/cm^2), θ/φ and Λ are the phase-matching angle and the period for degenerate operation at the given λ_P in birefringent and quasi phase-matching, respectively, and the GVM parameter $1/v_P$-$1/v_{S,I}$ is calculated for degenerate operation at λ_P.*

Crystal, interaction, plane	λ_P [μm]	λ_F [μm]	$\Delta\lambda$ [μm]	$\Delta\nu$ [THz]	θ/φ [°], Λ [μm]	$1/v_P$-$1/v_{S,I}$ [fs/mm]
KDP (e→oo)	0.492	1.035	0.818-1.233	366-243	41.3	94.5
PPSLT (e→ee)	0.561	1.660	0.966-1.338	311-224	9.1	577
LBO (e→oo) x-y	0.599	1.260	0.944-1.625	317-184	3.1	18.6
CLBO (e→oo)	0.629	1.339	0.995-1.710	301-175	27.7	9.94
BBO (e→oo)	0.716	1.547	1.121-1.982	267-151	19.95	15.0
BIBO (e→oo) x-z	0.790	1.637	1.228-2.139	244-140	11.05	11.4
BIBO (o→ee) x-z	0.805	1.723	1.275-2.184	235-137	35.4	31.6
PPKTP (e→ee)	0.894	2.505	1.511-2.188	198-137	32.4	141
$LiNbO_3$ (e→oo)	0.949	2.025	1.690-2.166	177-138	45.3	36.7
PPLN (e→ee)	0.956	2.686	1.705-2.176	176-137	27.9	165
$LiIO_3$ (e→oo)	0.970	2.231	1.609-2.940	186-102	18.7	31.5
$KNbO_3$ (e→oo) x-y	0.988	2.137	1.629-2.511	184-119	47.71	46.3
$KNbO_3$ (e→oo) y-z	1.004	2.066	1.656-2.550	181-117	15.63	17.5

*The Sellmeier and nonlinear coefficient data used for the table, with the exception of BIBO, is from Ref. 22: For KH_2PO_4 (KDP), LBO, $CsLiB_6O_{10}$ (CLBO), BBO, periodically poled KTP (PPKTP), $LiIO_3$, and $KNbO_3$, the so- called "best dispersion relations" were used; for $LiNbO_3$ and periodically poled lithium niobate (PPLN), the data chosen was for congruent material, and in the case of periodically poled stoichiometric $LiTaO_3$ (PPSLT) the data used was for stoichiometric lithium tantalate. The validity of the Sellmeier expansions does not always cover the full $\Delta\lambda$ ranges.

Similar arguments hold also for quasi-phase-matched materials where the turning point is defined with respect to the phase-matching period. Since in this case the polarization of the three waves is the same, one can expect that the deviation of λ_F from $2\lambda_P$ will be larger, see Fig. 3, leading to larger GVM with the pump. For instance, the GVM with the pump in the degenerate PPKTP-OPA pumped at the "magic" wavelength amounts to 141 fs/mm, it is 577 fs/mm in PPSLT while it is only 11.4 fs/mm in BIBO (e→oo).

Thus, it should be emphasized that in general there is nothing unique in the dispersive properties of BIBO concerning the achievable gain bandwidths, this concerns only the fact that from all existing crystals BIBO exhibits these important for collinear femtosecond OPAs/OPGs properties for a pump wavelength coinciding with the wavelength of the most widely

used and technologically developed ultrafast Ti:sapphire laser amplifiers. It can be seen from Table 2 that the achievable bandwidths in the four borates considered and in KDP, exceed 100 THz. However, as a result of the specific behavior of the three refractive indices of BIBO (presumably related to anomalous infrared dispersion) the two characteristic wavelengths λ_F and $2\lambda_P$ of BIBO are very close, especially for type e→oo phase-matching, which leads to low GVM between all the three waves in a degenerate OPA/OPG pumped near 800 nm.

The regime of ultrabroadband parametric generation has been realized before but using picosecond pump sources. Generation of WLC based on quadratic nonlinearity was demonstrated with an ultrabroadband OPG based on KDP as early as 1982,[23] achieving a spectral range of 90 THz. Ultrabroadband gain extending over 115 THz was demonstrated recently also with an OPG based on periodically poled KTP (PPKTP) pumped by 1 ps pulses.[24]

3. ULTRABROADBAND OPA BASED ON TYPE-I BIBO

The experimental set-up of the OPA is shown in Fig. 4. Since continua generated from 800 nm exhibit strongly decreasing intensity towards 1600 nm, we used as a seed the anti-Stokes part of the WLC generated at longer pump wavelengths. The OPA is pumped by a commercial (SPITFIRE, Spectra-Physics) Ti:sapphire amplifier system which provides pulses of 45 fs duration (Gaussian shape assumption) with an energy of up to 2 mJ. For the present experiment a total of 0.7 mJ was used, distributed among the OPG used to pump the WLC generator, the pump beam for the BIBO based OPA, and the probe beam (Fig. 4).

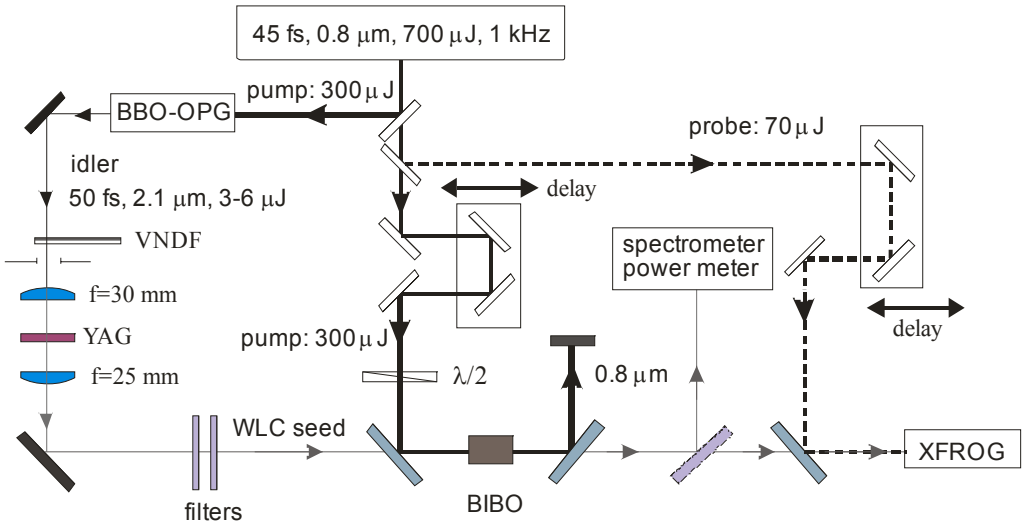

Fig. 4. Schematic of the experimental OPA set-up: VNDF: variable neutral density filter, filters: Ho:YAG mirrors reflecting the 2.1 μm pump, XFROG: cross-correlation FROG based on sum-frequency generation.

An additional BBO based OPG (TOPAS, Light Conversion Ltd.) was used as a pump source for the WLC continuum seed. The pulses at the idler wave near 2.1 μm had a duration of 50 fs (FWHM). Several microjoules were focused onto a 3-mm thick YAG plate. YAG was chosen because it combines high damage resistivity and nonlinear index of refraction, see Fig. 5. A variable neutral density filter was used to precisely adjust the pump level in order to obtain stable single filament. After recollimation, the 2.1-μm beam was blocked by reflecting Ho:YAG laser mirrors, and the WLC was recombined with the pump beam at 800 nm for the BIBO-OPA stage.

The uncoated 3- and 5-mm thick BIBO crystals employed in the OPA were cut at θ=11.4° in the *x*-*z* plane. The average pump intensity (½ of the peak on-axis level) at 800 nm was 60 GW/cm^2. Behind the crystals, the residual pump radiation was blocked by a mirror transmitting the amplified WLC which was then characterized by an InGaAs spectrometer and a power meter. Finally, using a fraction of the fresh pump beam as a probe (gate) pulse, XFROG (cross-correlation FROG based on sum-frequency generation in a 10 μm thick, type-I (oo→e) BBO crystal) measurements of the parametrically generated radiation were performed. The latter were used to reconstruct the entire spectrum and the integral pulse

duration for the amplified WLC as well as to obtain rough information about the phase-modulation. Care was taken to ensure collinear amplification in the BIBO crystals.

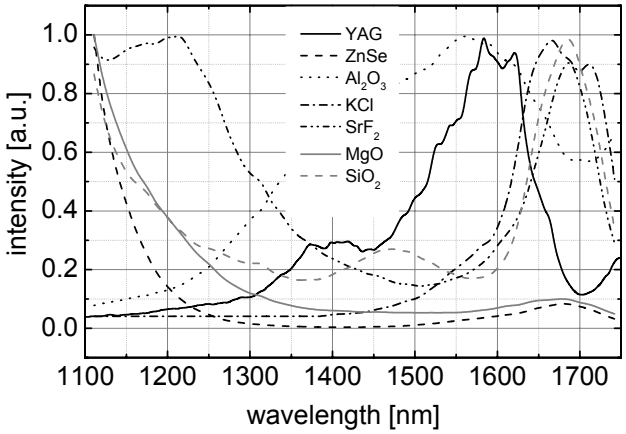

Fig. 5. Calibrated and normalized WLC spectra in the near-IR generated by single filamentation in different materials of 50 fs pulses at 2.1 μm.

Typical maximum energies of the amplified WLC achieved were 30 and 50 μJ for the 3- and 5-mm thick BIBO crystals, respectively. These values were obtained for pump delays which simultaneously provided ultrabroad bandwidths of the amplified WLC. Thus the maximum intrinsic conversion efficiency was 20% for the 5-mm thick BIBO. The amplified WLC spectra in the case of 3- and 5-mm thick BIBO are shown in Figs. 6a and b, respectively. The partial spectrum up to 1600 nm (thick solid curves) was directly recorded by an InGaAs-based spectrometer while the complete spectrum shown by dashed curves was reconstructed from the XFROG trace which was recorded with a VIS spectrometer, see Fig. 8. Finally, the thick grey curves in Fig. 6 show the portion of the amplified spectrum (>1600 nm) that was calculated from the one directly measured below 1600 nm, using the Manley-Rowe relation. The obtained amplification bandwidth was ~80 THz for the 3-mm thick BIBO, and it increased to ~100 THz in the case of the 5-mm thick BIBO.

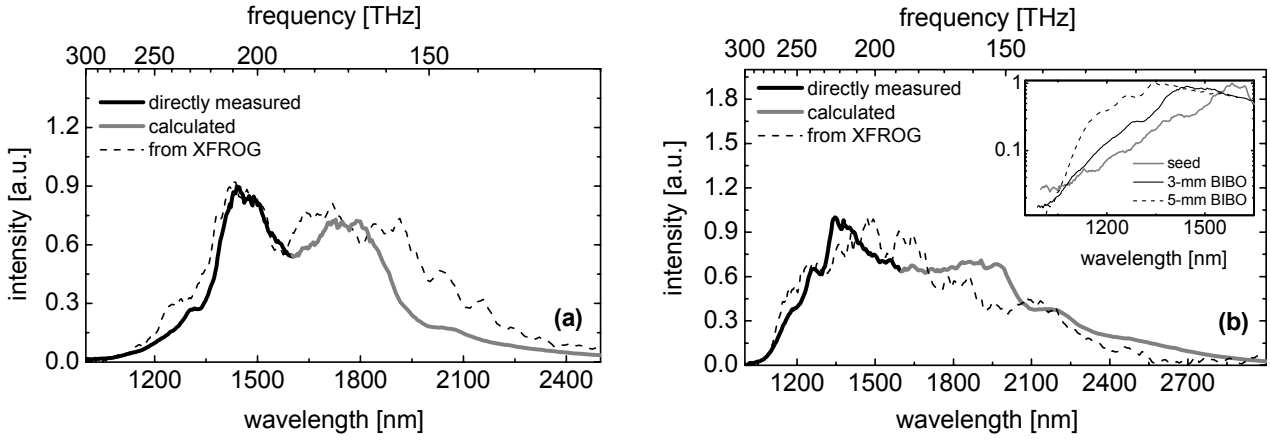

Fig. 6. Spectra of the WLC amplified in 3-mm (a) and 5-mm (b) thick BIBO: measured by the InGaAs spectrometer (thick solid curves), reconstructed from the time-integrated XFROG trace (dashed curves) and computed from the Manley-Rowe relation (grey curves). The inset in (b) is a comparison of the spectra of the WLC seed generated in YAG (grey line), and the amplified WLC in the 3-mm (solid line) and 5-mm (dashed line) thick BIBO crystals.

The FWHM of the cross correlation functions (Figs. 7a and b) recovered from the XFROG measurement were 84 and 105 fs for the 3- and 5-mm thick BIBO crystals, respectively, i.e. the corresponding amplified WLC pulse durations (FWHM intensity) are τ~70 fs and τ~95 fs, 1.4 and 1.9 times longer than the pump pulses at 2.1 μm, respectively. A

Gaussian pulse shape assumption was used for this rough estimation, the same as for the pump pulses. The time-bandwidth product amounts thus to 5.6 and 9.5 for the 3- and 5-mm thick BIBO crystals, respectively.

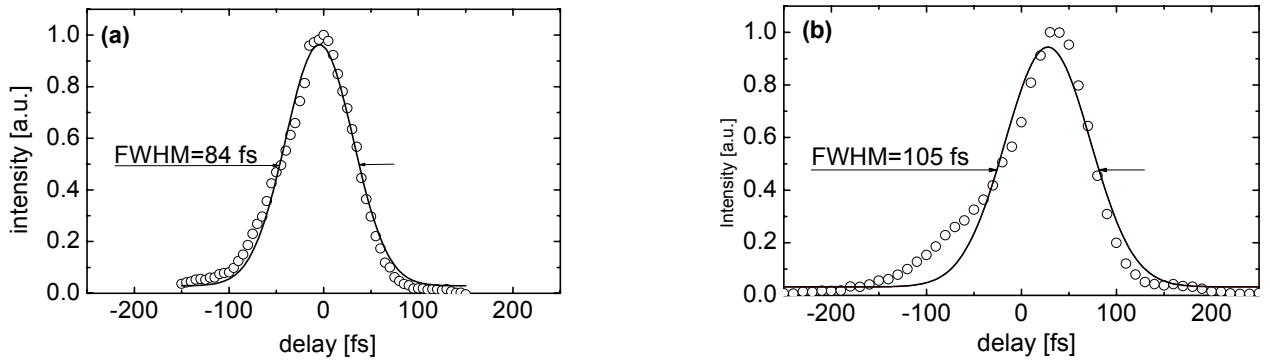

Fig. 7. Cross correlation functions with Gaussian fits of the amplified WLC in the 3-mm (a) and 5-mm (b) thick BIBO. The FWHM indicated corresponds to the Gaussian fits to the cross correlation traces.

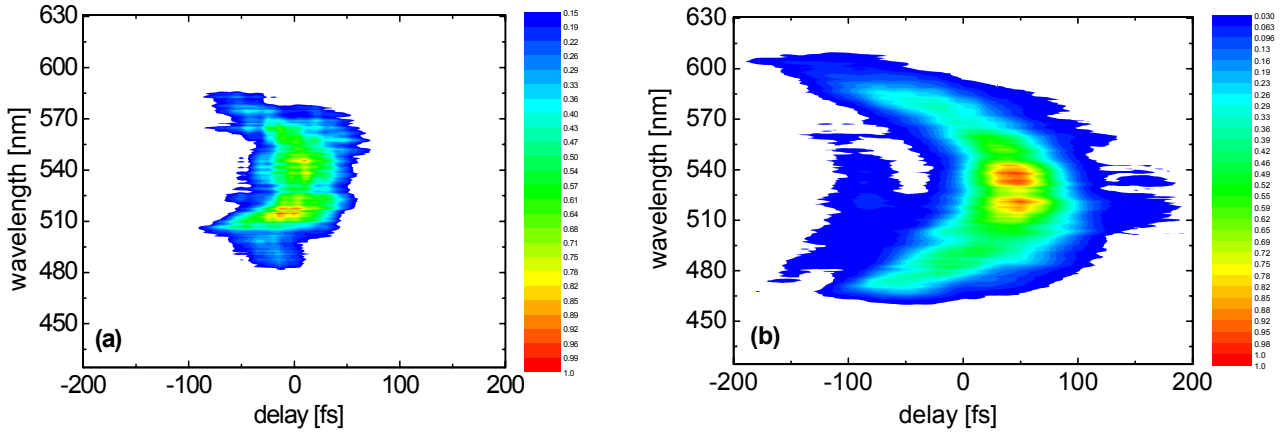

Fig. 8 XFROG traces of the WLC amplified in the 3-mm (a) and 5-mm (b) thick BIBO using probe pulses at 800 nm for the sum-frequency generation.

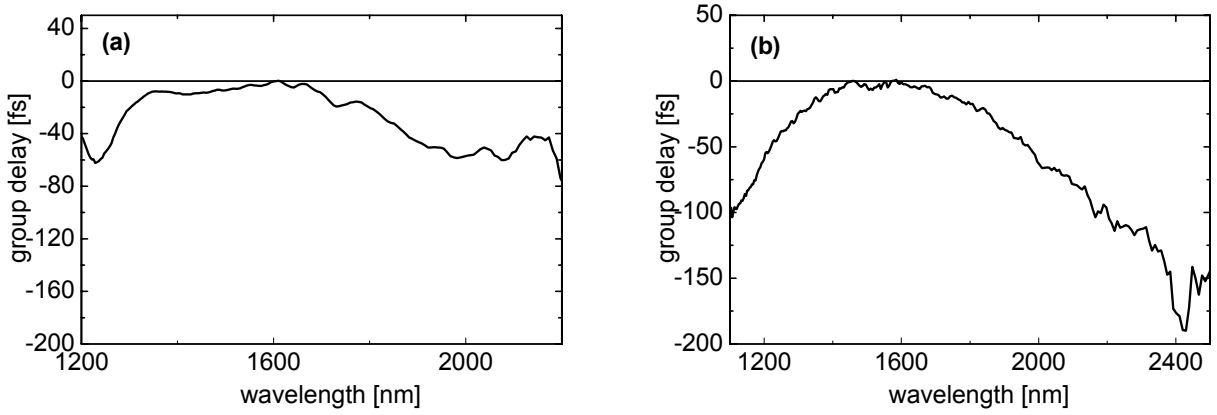

Fig. 9 Evaluation of the group delay versus wavelength for the 3-mm (a) and 5-mm (b) thick BIBO calculated from the XFROG traces in Fig. 8 using the center of gravity for each cross-section corresponding to a fixed sum-frequency wavelength.

The simultaneous increase of the spectral width and pulse duration for the longer BIBO crystal can only be explained by involving chirp effects. In that case the increasing temporal walk-off between the pump and amplified pulses results in spectral broadening. The WLC seed level did not allow the direct characterization of its temporal and spectral properties. However, from estimations of the GVD in all optical elements used (including the YAG and BIBO crystals) we conclude that the main source of chirp is the BIBO crystal itself. This is not unexpected since this material exhibits the lowest band-gap. Since the zero GVD point is near the 1600 nm degeneracy point, the chirp produced by GVD in BIBO has opposite sign for the signal and idler frequencies which can be seen in Fig. 9. While this satisfies the requirement for energy conservation in the case of OPA pumped by monochromatic pump it is clear that compensation of such chirp in subsequent pulse compression schemes will not be trivial.

4. ULTRABROADBAND OPG BASED ON TYPE-I BIBO

In the OPG experiments we studied the same two uncoated BIBO crystals of length 3 and 5 mm, using the same pump source with an incident pulse energy of 260 μJ but without seeding. The same diagnostics and analysis techniques were used as in the OPA case. Collinear output was analyzed only; in the case of OPG the non-collinear geometry is undesirable because different spectral components propagate in different directions.

Most of the measurements in this section were performed for average pump intensities of 100 GW/cm^2 for the 3-mm thick crystal and 60 GW/cm^2 for the 5-mm thick crystal. The WLC energies, measured after blocking the pump beam, were 8 and 12 μJ for the 3- and 5-mm long BIBO crystals, respectively. It was not possible to increase further the pump intensity in the case of the thicker sample because higher order nonlinear effects were observed (non-phase-matched continuum generation). However, with the shorter crystal, it was possible to raise the pump intensity to 150 GW/cm^2 without any detrimental effects. This led to a total output energy of 15 μJ. Taking into account the transmission of the optics used and the Fresnel reflections at the crystal faces, this corresponds to an internal conversion efficiency of ≈7%.

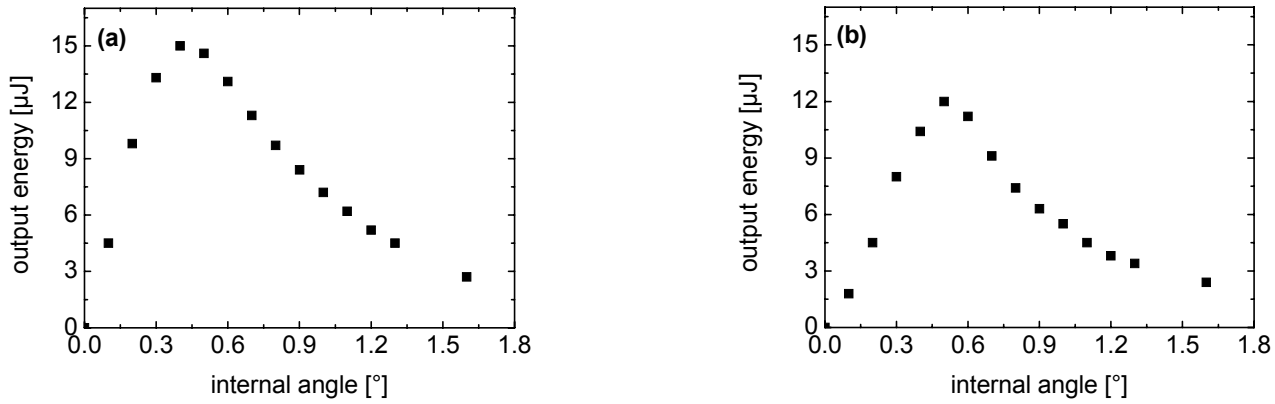

Fig. 10. OPG output energy obtained with the 3-mm (a) and 5-mm (b) thick BIBO crystals versus internal phase-matching angle relative to normal incidence. The average pump intensity (1/2 of the peak on-axis level) is 150 GW/cm^2 (a) and 60 GW/cm^2 (b).

Figures 10a and b show the measured OPG output energy for the 3 and 5-mm thick BIBO crystals, respectively, in dependence on the internal angle of the pump beam relative to the normal to the crystal surface. Increasing internal angle corresponds to decreasing phase-matching angle θ, however, direct relation is avoided here because of the inevitable inaccuracy of the crystal cut which could be of the same order as the angular changes studied. As can be expected, at some maximum phase-matching angle, in this case corresponding to almost normal incidence, there is no phase-matching and the output energy drops to zero.

Figures 11a and b show the OPG spectra, recorded for the 3 and 5-mm thick BIBO crystals. The dependence of the output spectra on the phase-matching angle is in agreement with the theoretical predictions for the parametric gain shown in Figs. 12a and b, which were calculated directly from Eq. (1). While the calculations for Fig. 2 and Table 2 were at exact phase-matching angle or period, here the phase-matching angle was varied for a fixed pump wavelength of

λ_P=800 nm. In contrast to the analytical approximation used in Fig. 1b, where the bandwidth is calculated only for the one wave assuming single peaked gain function, it can be seen from Fig. 12 that the actual gain bandwidth can be further increased when the spectral gain profiles for the signal and idler waves merge. Note that the phase-matching angle for which this happens is slightly lower than the one corresponding to degeneracy (θ=11.05° for λ_P=800 nm). The broadest parametric gain occurs before the two spectra have totally merged. It extends roughly from 1.15 to 2.4 µm. The additional enhancement of the bandwidth achieved in this way is up to ≈50% if compared to the values given in terahertz in Table 2. In fact the broadest parametric gain (depending on its definition, i.e. the acceptable dips in the spectral distribution) does not necessarily occur for the magic pump wavelength: Both the pump wavelength and the phase-matching angle can slightly deviate near the values specified in Table 2, to achieve maximum bandwidths.[24,25,26]

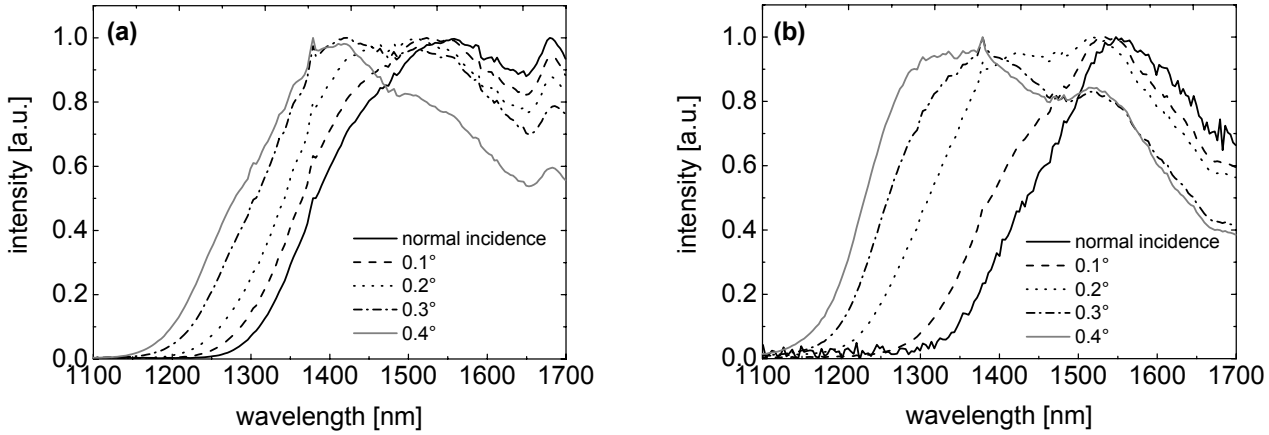

Fig. 11. OPG spectra obtained with the 3-mm (a) and 5-mm (b) thick BIBO crystals, recorded with an InGaAs spectrometer at five different internal angles of the pump beam. The pump intensity is 100 GW/cm^2 (a) and 60 GW/cm^2 (b).

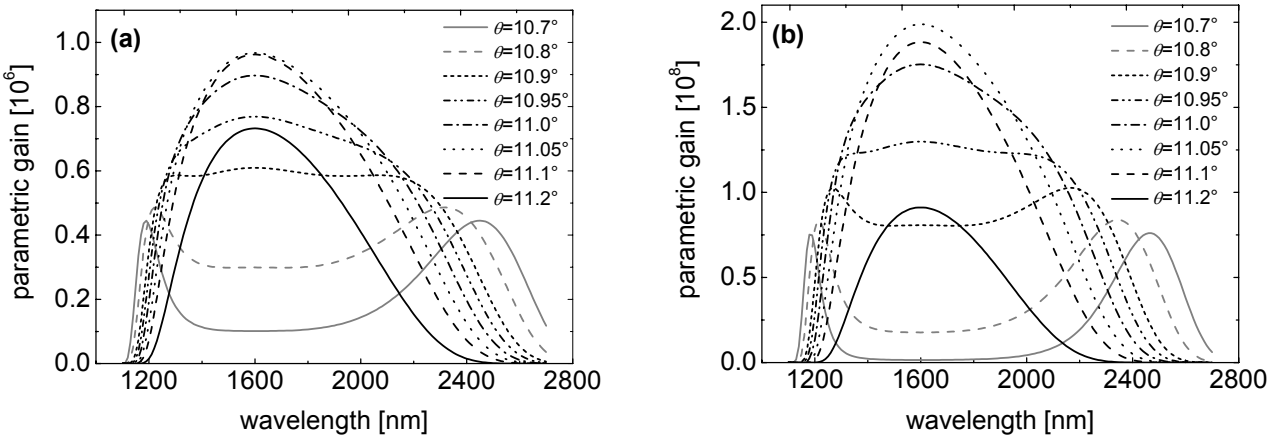

Fig. 12. Parametric gain of BIBO for collinear type e→oo interaction at λ_P=800 nm, calculated for several fixed phase-matching angles close to degeneracy (θ=11.05°). The crystal length, 3 mm (a) and 5 mm (b), and the pump intensity, 100 GW/cm^2 (a) and 60 GW/cm^2 (b), correspond to the experimental conditions in Fig. 11.

With increasing incidence angle in Fig. 11, the spectra gain in bandwidth, with the broadest spectrum at a relative internal angle of ≈0.4°, corresponding to the broadest parametric gain. With further increase of the incidence angle (decrease of the phase-matching angle θ) the spectra tend to be narrower again, as can be expected for a phase-matching angle deviating from the one corresponding to degeneracy. The main qualitative difference in the spectra obtained with the 3- and 5-mm long BIBO samples is the decreasing intensity above 1500 nm, observed only for the longer crystal. For the thinner crystal, the spectral intensity remains almost constant above 1500 nm up to the limit of detection of the InGaAs array. The spectral extension of the WLC is slightly larger for the 5-mm long BIBO crystal which can be

attributed to the increasing role of the GVM with the pump pulse, leading to chirp formation, as will be seen in the XFROG traces. However, having in mind the roughly 200 times higher gain in Fig. 12b in comparison to Fig. 12a, it can be concluded that in the spectral range where the spectral gain bandwidth is determined by higher order dispersion terms the effect of the gain coefficient Γ on it is rather weak.[19,23]

Figures 13-15 show the output spectra (a), the XFROG traces (b) and the cross-correlation functions with the gate pulse obtained by integration of the XFROG traces (c) for these three cases.

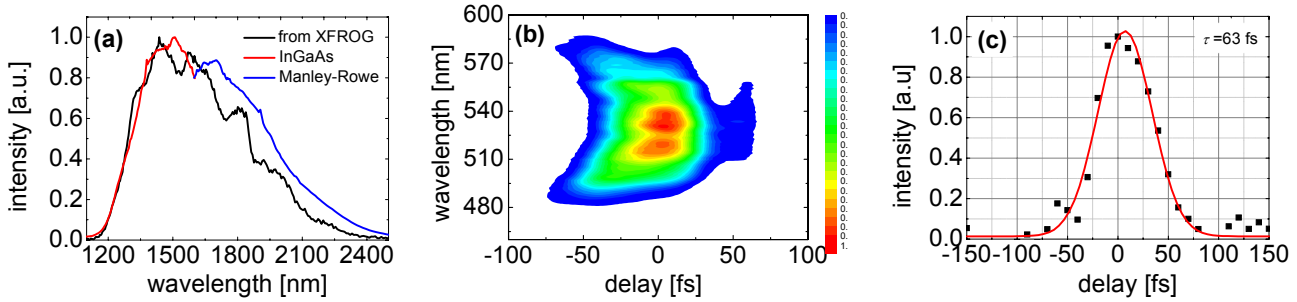

Fig. 13. Spectrum (a), XFROG trace (b) and cross-correlation function with Gaussian fit (c) of the OPG output with the 3-mm thick BIBO crystal; pump intensity: 100 GW/cm^2.

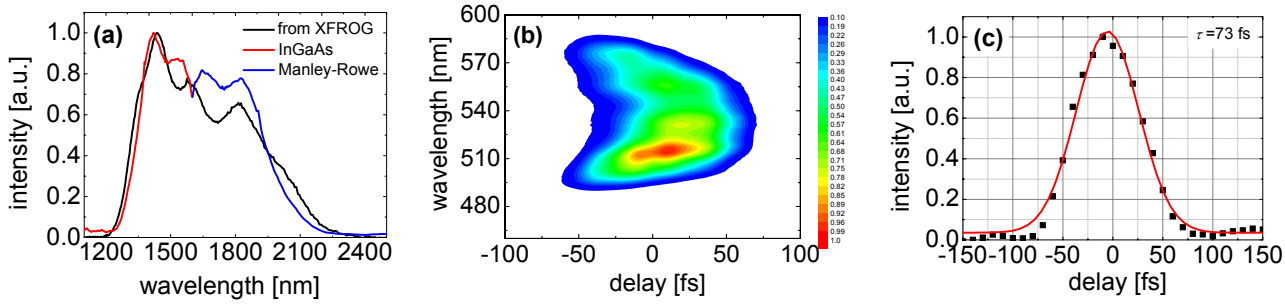

Fig. 14. Spectrum (a), XFROG trace (b) and cross-correlation function with Gaussian fit (c) of the OPG output with the 5-mm thick BIBO crystal; pump intensity: 60 GW/cm^2.

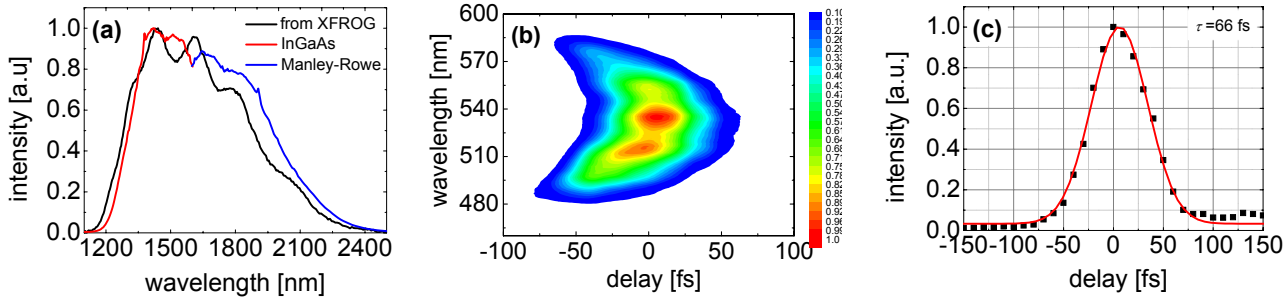

Fig. 15. Spectrum (a), XFROG trace (b) and cross-correlation function with Gaussian fit (c) of the OPG output with the 3-mm thick BIBO crystal; pump intensity: 150 GW/cm^2.

The spectral portions up to 1600 nm shown by the red curves in Figs. 13a-15a are from direct measurements with the InGaAs spectrometer. The black curves in the same figures show the spectra which were reconstructed from the XFROG traces recorded with a VIS spectrometer. Finally, the parts of the amplified spectra above 1600 nm, shown by blue lines in Figs. 13a-15a, were calculated using the Manley-Rowe relation. In all three cases the correspondence between the two methods used to recover the spectral information is rather satisfactory. Taking as a measure the spectra derived from the XFROG traces, the spectral extension of the generated WLC at the 0-level is roughly 135 THz in all the three cases.

As can be seen from Figs. 13c-15c, the integrated cross correlation functions are well fitted by Gaussian curves. Since the autocorrelation function of the pump pulses was also analyzed using such a pulse shape, we deconvolved the cross-correlation traces under the same assumption. The resulting integral WLC pulse durations are indicated in the figures as τ (FWHM intensity). The obtained pulse durations are shorter than in the OPA case. The shortest pulse duration, τ=63fs, was measured for the case of the 3-mm long crystal pumped at 100 GW/cm^2. As can be expected this occurs at the lowest conversion efficiency. The calculated time-bandwidth products are roughly 10 times above the Fourier limit for Gaussian pulse shapes: $\Delta\nu\tau\approx$4.2 for Fig. 13, ≈4.7 for Fig. 14, and ≈5 for Fig. 15.

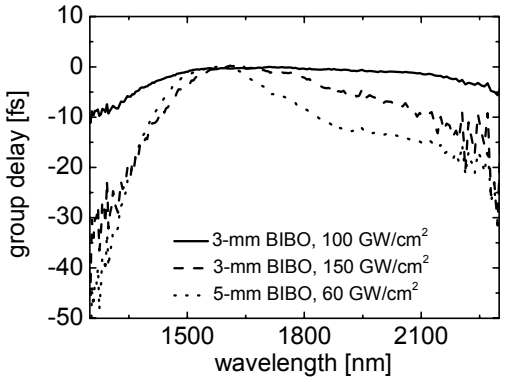

Fig. 16. Group delay derived from the XFROG traces for the three cases depicted in Figs. 13-15.

The shape of the XFROG traces in Figs. 13b-15b is similar to the one obtained in the analogous OPA experiments. In principle, this result confirms our estimations that the phase-modulation observed at the OPA output is not caused by the WLC generator or some passive optical elements but is rather due to the BIBO crystal itself. The same can be obviously expected in the OPG case. Since the zero GVD point is very close to the point separating the signal and idler branch, opposite chirp is observed in the two branches, see Fig. 16. On the other hand, opposite sign of the chirp is anyway a condition imposed by the energy conservation law in three-wave interactions, at least under the assumptions stated in section 2. The chirp is more pronounced with increasing parametric gain (conversion efficiency).

Finally, we performed an additional series of experiments to establish the effect of the pump pulse duration on the OPG performance. An analogous pump source at 800 nm, delivering pulses of 100 fs duration was employed. Typical pump energies incident on the crystals were 300 μJ. At similar pump intensities the energy output from both, the 3-mm thick and the 5-mm thick BIBO crystals was doubled. In terms of spectral bandwidth, pulse duration, and time-bandwidth products, the results were similar to those described above. The integral pulse durations in this case were shorter than the pump pulses and the chirp was not pronounced.

5. CONCLUSION

In conclusion, the monoclinic crystal BIBO possesses a unique combination of excellent properties for broadband parametric amplification when pumped near 800 nm in collinear geometry. Higher order dispersion terms determine in this case the parametric gain bandwidth which can be extremely broad. In addition, the group velocity matching with the pump ensures long interaction lengths and high efficiency even for femtosecond pulse durations. Hence, BIBO is a very promising candidate for a wide range of femtosecond down-conversion schemes based on Ti:sapphire laser pump sources. We have demonstrated ultrabroadband optical parametric amplification and generation in the near-IR with WLC energy as high as 50 μJ in the case of OPA and 15 μJ in the case of the simpler OPG scheme. These values correspond to internal conversion efficiency of 20% and 7%, respectively. In all cases the integral pulse durations achieved are in the sub-100-fs range and the spectral extension covers an octave. This is the first time such WLC has been generated or amplified by a second order nonlinear process on the femtosecond time scale.

Two main conclusions can be drawn from the shape of the measured XFROG traces and the chirp behavior: (i) The fact that the zero GVD point separates the signal and idler spectral ranges is not favorable for amplification of linearly chirped WLC with subsequent compression because normally the BIBO crystal itself is the main source of chirp. Hence, the direct generation of few cycle pulses, as supported from the observed bandwidths cannot profit from the amplification of WLC, the situation in a BIBO based OPG is similar. (ii) Compression of the output pulses in order to reduce the time-bandwidth product and obtain few cycle pulses should be in principle possible but will require more sophisticated schemes than a simple prism or grating compressor. Chirped mirrors or adaptive compressors could be some alternatives. However, spectral selection of the signal or idler branch from the OPG spectra could be feasible to produce sub-20 fs pulses with microjoule energy using a simple compressor to compensate the quadratic phase term.

Further investigation of the temporal modification of the WLC characteristics in the BIBO based OPAs and OPGs will require gate pulses with duration shorter than that of the pump pulses to be used in the XFROG analysis or the use of second harmonic FROG.

ACKNOWLEDGMENT

We acknowledge financial support from the German-Bulgarian exchange programme (DAAD grant D/05/11319 and Bulgarian Ministry of Education and Science grants D01-81/2006 and D01-619/2007).

REFERENCES

[1] P. Tzankov and V. Petrov, "Effective second-order nonlinearity in acentric optical crystals with low symmetry," Appl. Opt. **44**, 6971-6985, 2005.

[2] H. Hellwig, J. Liebertz, and L. Bohaty, „Exceptional large nonlinear optical coefficients in the monoclinic bismuth borate BiB_3O_6 (BIBO)," Solid State Commun. **109**, 249-251, 1999.

[3] Zh. Lin, Zh. Wang, C. Chen, and M.-H. Lee, "Mechanism for linear and nonlinear optical effects in monoclinic bismuth borate (BiB_3O_6) crystal," J. Appl. Phys. **90**, 5585-5590, 2001.

[4] H. Hellwig, J. Liebertz, and L. Bohaty, „Linear optical properties of the monoclinic bismuth borate BiB_3O_6," J. Appl. Phys. **88**, 240-244, 2000.

[5] M. Ebrahim-Zadeh, "Ultrafast frequency conversion sources for the visible and ultraviolet based on BiB_3O_6," Proc. SPIE **6451**, 645106-1-15, 2007.

[6] V. Petrov, M. Ghotbi, P. Tzankov, F. Noack, I. Nikolov, I. Buchvarov, and M. Ebrahim-Zadeh, "Optical parametric generation of high-energy femtosecond pulses in the 1-3 μm spectral range using BiB_3O_6," Proc. SPIE **6455**, 64550C-1-12, 2007.

[7] M. Ebrahim-Zadeh, "Efficient ultrafast frequency conversion sources for the visible and ultraviolet based on BiB_3O_6," IEEE J. Sel. Top. Quantum Electron. **13**, 679-691, 2007.

[8] M. Ghotbi, M. Ebrahim-Zadeh, A. Majchrowski, E. Michalski, and I. V. Kytik, "High-average-power femtosecond pulse generation in the blue using BiB_3O_6," Opt. Lett. **29**, 2530-2532, 2004.

[9] M. Ghotbi and M. Ebrahim-Zadeh, "Optical second harmonic generation properties of BiB_3O_6," Opt. Exp. **12**, 6002-6019, 2004.

[10] T. Harimoto, Y. Takeuchi, and M. Fujita, "Spectral properties of second-harmonic generation at 800 nm in a BiB_3O_6 crystal," Opt. Exp. **12**, 811-816, 2004.

[11] M. Ghotbi, A. Esteban-Martin, and M. Ebrahim-Zadeh, "Tunable high-repetition-rate femtosecond pulse generation in the ultraviolet with BiB_3O_6," Conference on Lasers and Electro-Optics CLEO'06, Long Beach (CA), USA, May 21-26, 2006, paper JThC70, CLEO/QELS Technical Digest CD-ROM.

[12] M. Ghotbi, A. Esteban-Martin, and M. Ebrahim-Zadeh, "BiB_3O_6 femtosecond optical parametric oscillator," Opt. Lett. **31**, 3128-3130, 2004.

[13] M. Ghotbi, A. Esteban-Martin, and M. Ebrahim-Zadeh, "Ti:sapphire-pumped infrared femtosecond optical parametric oscillator based on BiB_3O_6," Conference on Lasers and Electro-Optics CLEO'07, Baltimore (MD), USA, May 6-11, 2007, paper JWA31, CLEO/QELS Technical Digest CD-ROM.

[14] M. Ghotbi, M. Ebrahim-Zadeh, V. Petrov, P. Tzankov, and F. Noack, "Efficient 1 kHz femtosecond optical parametric amplification in BiB_3O_6 pumped at 800 nm," Opt. Exp. **14**, 10621-10626, 2006.

[15] V. Petrov, F. Noack, P. Tzankov, M. Ghotbi, M. Ebrahim-Zadeh, I. Nikolov, and I. Buchvarov, "High-power femtosecond optical parametric amplification at 1 kHz in BiB_3O_6 pumped at 800 nm," Opt. Exp. **15**, 556-563, 2007.

[16] N. Umemura, K. Miyata, and K. Kato, "New data on the optical properties of BiB_3O_6," Opt. Mat. **30**, 532-534, 2007.

[17] R. Danielius, A. Piskarskas, A. Stabinis, G. P. Banfi, P. Di Trapani, and R. Righini, „Traveling-wave parametric generation of widely tunable, highly coherent femtosecond light pulses," J. Opt. Soc. Am. **10**, 2222-2232, 1993.

[18] G. Cerullo and S. De Silvestri, „Ultrafast optical parametric amplifiers," Rev. Sci. Instrum. **74**, 1-18, 2003.

[19] A. Birmontas, A. Piskarskas, and A. Stabinis, "Dispersion anomalies of tuning characteristics and spectrum of an optical parametric oscillator," Sov. J. Quantum Electron. **13**, 1243-1246, 1983 [transl. from Kvantovaya Elektron. (Moscow) **10**, 1881-1884, 1983].

[20] X. Liu, D. Deng, M. Li, D. Guo, and Z. Xu, "Retracing behaviour of the phase-matching angle of nonlinear crystals in optical parametric oscillators," J. Appl. Phys. **74**, 2989-2991, 1993.

[21] M. S. Webb, D. Eimerl, and S. P. Velsko, "Wavelength insensitive phase-matched second-harmonic generation in partially deuterated KDP," J. Opt. Soc. Am. B **9**, 1118-1127, 2007.

[22] D. N. Nikogosyan, "Nonlinear optical crystals," Springer, New York, 2005.

[23] B. Bareika, A. Birmontas, G. Dikchyus, A. Piskarskas, V. Sirutkaitis, and A. Stabinis, "Parametric generation of picosecond continuum in near-infrared and visible ranges on the basis of a quadratic nonlinearity," Sov. J. Quantum Electron. **12**, 1654-1656, 1982 [transl. from Kvantovaya Elektron. (Moscow) **9**, 2534-2536, 1982].

[24] M. Tiihonen, V. Pasiskevicius, A. Fragemann, C. Canalias, and F. Laurell, "Ultrabroadband gain in optical parametric generator with periodically poled $KTiOPO_4$," Appl. Phys. B **85**, 73-77, 2006.

[25] S. N. Orlov, E. V. Pestryakov, and Yu. N. Polivanov, "Optical parametric amplification with bandwidth exceeding an octave," Quantum Electron. **34**, 477-479, 2004 [transl. from Kvantovaya Elektron. (Moscow) **34**, 477-481, 2004].

[26] P. Tzankov, I. Buchvarov, and T. Fiebig, "Broadband optical parametric amplification in the near UV-VIS," Opt. Commun. **203**, 107-113, 2002.